

An efficient and highly accurate solver for multi-body acoustic scattering problems involving rotationally symmetric scatterers

S. Hao, P.G. Martinsson, P. Young

Abstract: A numerical method for solving the equations modeling acoustic scattering in three dimensions is presented. The method is capable of handling several dozen scatterers, each of which is several wave-lengths long, on a personal work station. Even for geometries involving cavities, solutions accurate to seven digits or better were obtained. The method relies on a Boundary Integral Equation formulation of the scattering problem, discretized using a high-order accurate Nyström method. A hybrid iterative/direct solver is used in which a local scattering matrix for each body is computed, and then GMRES, accelerated by the Fast Multipole Method, is used to handle reflections between the scatterers. The main limitation of the method described is that it currently applies only to scattering bodies that are rotationally symmetric.

1. INTRODUCTION

The manuscript presents a robust and highly accurate numerical method for modeling frequency domain acoustic scattering on a domain external to a group of scatterers in three dimensions. The solver is designed for the special case where each scatterer is rotationally symmetric, and relies on a Boundary Integral Equation (BIE) formulation of the scattering problem.

The contribution of the manuscript is to combine several recently developed techniques to obtain a solver capable of solving scattering problems on complex multibody geometries in three dimensions to seven digits of accuracy or more. In particular, the solver is capable of resolving domains involving cavities such as, e.g., the geometry shown Figure 5(a).

The solution technique proposed involves the following steps:

- (1) *Reformulation.* The problem is written mathematically as a BIE on the surface of the scattering bodies using the “combined field” formulation [5, 19]. See Section 2 for details.
- (2) *Discretization.* The BIE is discretized using the Nyström method based on a high-order accurate composite Gaussian quadrature rule. Despite the fact that the kernel in the BIE is singular, high accuracy can be maintained using the correction techniques of [16, 13]. Following [20], we exploit the rotational symmetry of each body to decouple the local equations as a sequence of equations defined on a generating contour [22, 23, 17, 25, 24]. This dimension reduction technique requires an efficient method for evaluating the fundamental solution of the Helmholtz equation in cylindrical coordinates (the so called “toroidal harmonics”); we use the technique described in [26]. See Section 3 for details.
- (3) *Iterative solver.* The dense linear system resulting from the Nyström discretization of the BIE is solved using the iterative solver GMRES [21], combined with a block-diagonal pre-conditioner, as in, e.g., [15, Sec. 6.4]. This pre-conditioner exploits that a highly accurate discrete approximation to the scattering matrix for each individual scatterer can be computed efficiently. See Section 4 for details.
- (4) *Fast matrix-vector multiplication.* The application of the coefficient matrix in the iterative solver is accelerated using the Fast Multipole Method (FMM) [10], specifically the version for the Helmholtz equation developed by Gimbutas and Greengard [8].
- (5) *Skeletonization.* In situations where the individual scatterers are not packed very tightly, the number of degrees of freedom in the global system can be greatly reduced by exploiting rank deficiencies in the off-diagonal blocks of the coefficient matrix. Specifically, we use a variation of the scheme introduced in [3], and further developed in [18]. Randomized methods are used to accelerate the computation of low-rank approximations to large dense matrices [12]. See Section 5 for details.

The present work draws on several recent papers describing techniques for multibody scattering, including [15], which applies a very similar technique to acoustic scattering in two dimensions. [9] addresses the harder problem of electro-magnetic scattering in 3D (as opposed to the acoustic scattering considered here), but uses classical scattering matrices expressed in spherical harmonics. This is a more restrictive frame-work than the one used in [15] for problems in 2D, and in the present work for problems in 3D. The more general model for a compressed scattering matrix that we use here allows for larger scatterers to be handled, and also permits it to handle scatterers closely packed together. For a deeper discussion of different ways of representing compressed scattering matrices, see [2].

To describe the asymptotic cost of the method presented, let m denote the number of scatterers, let n denote the total number of discretization nodes on a single scatterer and let I denote the number of iterations required in our pre-conditioned iterative solver to achieve convergence. The cost of building all local scattering matrices is then $O(mn^2)$, and the cost of solving the linear system consists of the time T_{FMM} required for applying the coefficient matrices using the FMM, and the time T_{precond} required for applying the block-diagonal preconditioner. These scale as $T_{\text{FMM}} \sim Imn$ and $T_{\text{precond}} \sim Imn^{3/2}$ (cf. Remark 4), but for practical problem sizes, the execution time is completely dominated by the FMM. For this reason, we implemented a “skeletonization” compression scheme [3] that reduces the cost of executing the FMM from Imn to Imk , where k is a numerically determined “rank of interaction”. We provide numerical examples in Section 6 that demonstrate that when the scatterers are moderately well separated, k can be smaller than n by one or two orders of magnitude, leading to dramatic practical acceleration.

2. MATHEMATICAL FORMULATION OF THE SCATTERING PROBLEM

Let $\{\Gamma_p\}_{p=1}^m$ denote a collection of m smooth, disjoint, rotationally symmetric surfaces in \mathbb{R}^3 , let $\Gamma = \cup_{p=1}^m \Gamma_p$ denote their union, and let Ω denote the domain exterior to Γ . Our task is to compute the “scattered field” u generated by an incident field v that hits the scattering surface Γ , see Figure 1. For concreteness, we consider the so called “sound-soft” scattering problem

$$(1) \quad \begin{cases} -\Delta u(\mathbf{x}) - \kappa^2 u(\mathbf{x}) = 0 & \mathbf{x} \in \Omega^c, \\ u(\mathbf{x}) = -v(\mathbf{x}) & \mathbf{x} \in \Gamma, \\ \frac{\partial u(\mathbf{x})}{\partial r} - i\kappa u(\mathbf{x}) = O(1/r) & r := |\mathbf{x}| \rightarrow \infty. \end{cases}$$

We assume that the “wave number” κ is a real non-negative number. It is known [5] that (1) has a unique solution for every incoming field v .

Following standard practice, we reformulate (1) as second kind Fredholm Boundary Integral Equation (BIE) using a so called “combined field technique” [5, 19]. We then look for a solution u of the form

$$(2) \quad u(\mathbf{x}) = \int_{\Gamma} G_{\kappa}(\mathbf{x}, \mathbf{x}') \sigma(\mathbf{x}') dA(\mathbf{x}'), \quad \mathbf{x} \in \Omega^c,$$

where G_{κ} is a combination of the single and double layer kernels,

$$(3) \quad G_{\kappa}(\mathbf{x}, \mathbf{x}') = \frac{\partial \phi_{\kappa}(\mathbf{x}, \mathbf{x}')}{\partial \mathbf{n}(\mathbf{x}')} + i\kappa \phi_{\kappa}(\mathbf{x}, \mathbf{x}')$$

and where ϕ_{κ} is the free space fundamental solution

$$(4) \quad \phi_{\kappa}(\mathbf{x}, \mathbf{x}') = \frac{e^{i\kappa|\mathbf{x}-\mathbf{x}'|}}{4\pi|\mathbf{x}-\mathbf{x}'|}.$$

Equation (2) introduces a new unknown function σ , which we refer to as a “boundary charge distribution”. To obtain an equation for σ , we take the limit in (2) as \mathbf{x} approaches the boundary

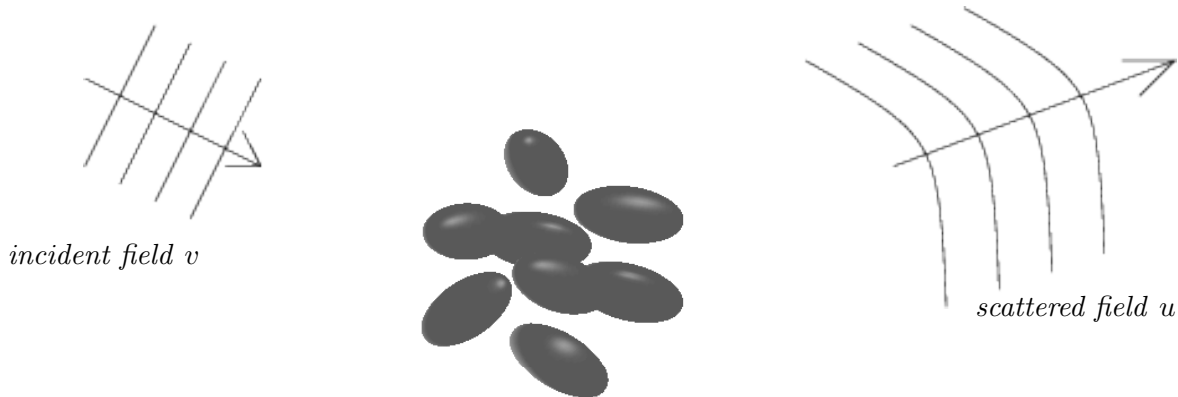


FIGURE 1. Geometry of scattering problem. An incident field v propagates in a medium with constant wave-speed and hits a scattering surface $\Gamma = \bigcup_{p=1}^m \Gamma_p$ (shown for $m = 8$). A charge distribution σ is induced on the surface Γ and generates an outgoing field u .

Γ , and find that σ must satisfy the integral equation

$$(5) \quad \frac{1}{2}\sigma(\mathbf{x}) + \int_{\Gamma} G_{\kappa}(\mathbf{x}, \mathbf{x}') \sigma(\mathbf{x}') dA(\mathbf{x}') = -v(\mathbf{x}), \quad \mathbf{x} \in \Gamma.$$

The combined field equation (5) is known to be a second kind Fredholm equation whenever Γ is smooth. Like the original boundary value problem (1), it is known to be well posed for every κ , see [5, Theorem. 3.9], [19, Sec. 3.2.2] (in particular, it does not suffer from the problem of “artificial resonances” that plague many alternative formulations).

3. DISCRETIZATION OF ROTATIONALLY SYMMETRIC SCATTERING BODIES

In Section 2 we formulated the scattering problem as the BIE (5) defined on the scattering surface Γ . In this section, we show how to discretize (5) to obtain a system of linear algebraic equations $\mathbf{A}\boldsymbol{\sigma} = -\mathbf{v}$. We use a Nyström technique that combines high accuracy, and (relative) ease of implementation. Section 3.1 gives a general overview of the Nyström method, Section 3.2 describes how rotational symmetry can be exploited to relatively easily discretize a single body to high order, and then Section 3.3 describes how to generalize the procedure to a multibody scattering problem.

3.1. Nyström discretization. The Nyström method provides a way of discretizing a BIE on a surface Γ from a quadrature rule for the surface that is valid for smooth functions. To illustrate, suppose that we are given *nodes* $\{\mathbf{x}_i\}_{i=1}^n$ and *weights* $\{w_i\}_{i=1}^n$ such that

$$(6) \quad \int_{\Gamma} \varphi(\mathbf{x}) dS(\mathbf{x}) \approx \sum_{i=1}^n \varphi(\mathbf{x}_i) w_i, \quad \text{for } \varphi \text{ smooth.}$$

The idea is then to first use the discretization nodes $\{\mathbf{x}_i\}_{i=1}^n$ as collocation points; in other words, we require that

$$(7) \quad \frac{1}{2}\sigma(\mathbf{x}_i) + \int_{\Gamma} G_{\kappa}(\mathbf{x}_i, \mathbf{x}') \sigma(\mathbf{x}') dA(\mathbf{x}') = -v(\mathbf{x}_i), \quad i = 1, 2, 3, \dots, n.$$

Next, suppose that we can somehow (this can require some work) construct an $n \times n$ matrix \mathbf{A} such that for any sufficiently smooth function φ , the integral in (7) can be approximated from

the function values $\{\sigma(\mathbf{x}_i)\}_{i=1}^n$

$$(8) \quad \frac{1}{2}\sigma(\mathbf{x}_i) + \int_{\Gamma} G_{\kappa}(\mathbf{x}_i, \mathbf{x}') \sigma(\mathbf{x}') dA(\mathbf{x}') \approx \sum_{j=1}^n A(i, j) \sigma(\mathbf{x}_j) \quad \text{for } \sigma \text{ smooth.}$$

Then a system of n equations for the n unknowns $\{\sigma(\mathbf{x}_i)\}_{i=1}^n$ is obtained by inserting the approximation (8) into (7). Specifically, given a data vector $\mathbf{v} \in \mathbb{C}^n$ given by $\mathbf{v}(i) = v(\mathbf{x}_i)$, we seek to determine a vector $\boldsymbol{\sigma} \in \mathbb{C}^n$ of approximations $\boldsymbol{\sigma}(i) \approx \sigma(\mathbf{x}_i)$ by solving the linear system

$$(9) \quad \sum_{j=1}^n A(i, j) \boldsymbol{\sigma}(j) = -\mathbf{v}(i), \quad i = 1, 2, 3, \dots, n.$$

The task of constructing a matrix \mathbf{A} such that (8) holds is complicated by the fact that the kernel $G_{\kappa}(\mathbf{x}, \mathbf{x}')$ has a singularity as $\mathbf{x}' \rightarrow \mathbf{x}$. Had this not been the case, one could simply have applied the rule (6) to the integral in (7) to obtain

$$(10) \quad A(i, j) = G_{\kappa}(\mathbf{x}_i, \mathbf{x}_j) w_j.$$

In Sections 3.2 and 3.3 we will describe how to construct a basic quadrature rule $\{\mathbf{x}_i, w_i\}_{i=1}^n$ that is suitable for the geometry under consideration, and also how to construct a matrix \mathbf{A} such that (8) holds to high accuracy despite the singular kernel. It turns out to be possible to do so while having almost all elements of \mathbf{A} given by the simple formula (10) — only matrix elements $A(i, j)$ for which $\|\mathbf{x}_i - \mathbf{x}_j\|$ is “small” need to be modified. As we will see in Section 4, this will greatly help when forming fast algorithms for evaluating the matrix-vector product $\boldsymbol{\sigma} \mapsto \mathbf{A}\boldsymbol{\sigma}$.

3.2. A single rotationally symmetric scatterer. We first consider the case where the scattering surface Γ is a single rotationally symmetric surface. We let γ denote a generating curve of Γ , and can then view Γ as a tensor product between γ and the circle \mathbb{T} , so that $\Gamma = \gamma \times \mathbb{T}$, see Figure 2. The idea is now to use a composite Gaussian rule to discretize γ , and a trapezoidal rule with equispaced nodes to discretize \mathbb{T} , and then take the tensor product between these rules to obtain the global rule $\{\mathbf{x}_i, w_i\}_{i=1}^n$ for Γ .

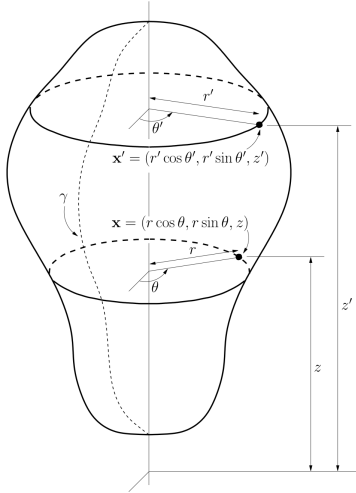


FIGURE 2. The axisymmetric domain Γ generated by the curve γ .

Remark 1 (Convergence order). *Suppose that φ is a smooth (C^∞) function on Γ . Then since φ is periodic in the azimuthal direction, the Trapezoidal rule converges super-algebraically fast. If we use p -point Gaussian quadrature on r intervals to discretize the generating curve γ , then the error in (6) scales as $(1/r)^{2p-1}$ as $r, p \rightarrow \infty$.*

The technique for constructing a matrix \mathbf{A} such that (8) holds is based on the observation that when Γ is a rotationally symmetric surface, the equation (5) is diagonalized by the Fourier transform. The process is somewhat involved and we will here give only a brief overview of the key techniques, for details we refer to [26]. The first step is to introduce cylindrical coordinates $\mathbf{x} = (r, \theta, z)$ with the z -axis being the symmetry axis of Γ , and let v_p , σ_p , and $G_{\kappa,p}$ denote the Fourier coefficients of the functions v , σ , and G_κ :

$$(11) \quad v(\mathbf{x}) = \sum_{p \in \mathbb{Z}} \frac{e^{ip\theta}}{\sqrt{2\pi}} v_p(r, z),$$

$$(12) \quad \sigma(\mathbf{x}) = \sum_{p \in \mathbb{Z}} \frac{e^{ip\theta}}{\sqrt{2\pi}} \sigma_p(r, z),$$

$$(13) \quad G_\kappa(\mathbf{x}, \mathbf{x}') = G_\kappa(\theta - \theta', r, z, r', z') = \sum_{p \in \mathbb{Z}} \frac{e^{ip(\theta - \theta')}}{\sqrt{2\pi}} G_{\kappa,p}(r, z, r', z').$$

Then (5) is equivalent to the sequence of equations

$$(14) \quad \frac{1}{2} \sigma_p(\mathbf{y}) + \sqrt{2\pi} \int_\gamma G_{\kappa,p}(\mathbf{y}, \mathbf{y}') \sigma_p(\mathbf{y}') dA(\mathbf{y}') = -v_p(\mathbf{y}), \quad \mathbf{y} \in \gamma, p \in \mathbb{Z}.$$

Converting the BIE (5) defined on a surface Γ to the sequence of BIEs (14) defined on the curve γ has a crucial advantage in that constructing high-order Nyström discretizations of BIEs with weakly singular kernels is well-understood and computationally cheap for curves, but remains a challenge for surfaces. We use the modified quadrature of [16], as described in [26, 13].

Beyond ease of discretization, the other key benefit of the formulation (14) is that for each Fourier mode p , the coefficient matrix arising from discretization of (14) is small enough that it can often easily be inverted by brute force. For instance, for the geometries shown in Figure 3, it is sufficient to use at most a couple of hundred nodes along γ to achieve ten digits accuracy. To put it another way, the Fourier conversion allows to write the matrix \mathbf{A} as a product

$$(15) \quad \mathbf{A} = \mathbf{F}^* \tilde{\mathbf{A}} \mathbf{F}$$

where \mathbf{F} is the discrete Fourier transform (in the azimuthal variable), and $\tilde{\mathbf{A}}$ is a block-diagonal matrix, where each diagonal block corresponds to one Fourier mode, and is relatively small. We can pre-compute and store the block diagonal matrix $\tilde{\mathbf{A}}^{-1}$, and then very rapidly apply the inverse

$$(16) \quad \mathbf{A}^{-1} = \mathbf{F}^* \tilde{\mathbf{A}}^{-1} \mathbf{F},$$

by using the FFT to apply \mathbf{F} and \mathbf{F}^* .

One complication to the procedure outlined in this section is that while the kernel G_κ in (5) is given by the simple formula (3), the kernels $G_{\kappa,p}$ must be evaluated computationally. Techniques for doing so rapidly have been developed, and are described in [26].

Remark 2 (Cost of precomputation). *To state the asymptotic cost of the algorithm, let N_G (“G” for Gaussian) denote the number of points on the generating curve γ of each scatter and let N_F (“F” for Fourier) denote the number of points used to discretize \mathbb{T} . The total number of degrees of freedom of each scatter is $n = N_G N_F$. Under the simplifying assumption that $N_G \sim N_F$, the cost of forming the block diagonal matrix $\tilde{\mathbf{A}}$ is $O(n^{3/2} \log n)$, while the cost of inverting $\tilde{\mathbf{A}}$ is $O(n^2)$, see [26]. Applying \mathbf{F} and \mathbf{F}^* is done via the FFT in negligible time.*

3.3. Multibody scattering. Having described how to discretize the single-body scattering problem in Section 3.2, we now proceed to the general case of m disjoint scattering surfaces $\Gamma = \cup_{p=1}^m \Gamma_p$. We assume that each scatterer is discretized using the tensor product procedure described in Section 3.2. For notational simplicity, we assume that each scatterer is discretized using the same n number of nodes, for a total of $N = mn$ discretization nodes $\{\mathbf{x}_i\}_{i=1}^N$ with associated weights $\{w_i\}_{i=1}^N$. We then seek to construct matrix blocks $\{\mathbf{A}_{p,q}\}_{p,q=1}^m$ such that the Nyström discretization of (5) associated with this quadrature rule takes the form

$$(17) \quad \begin{bmatrix} \mathbf{A}_{1,1} & \mathbf{A}_{1,2} & \cdots & \mathbf{A}_{1,m} \\ \mathbf{A}_{2,1} & \mathbf{A}_{2,2} & \cdots & \mathbf{A}_{2,m} \\ \vdots & \vdots & & \vdots \\ \mathbf{A}_{m,1} & \mathbf{A}_{m,2} & \cdots & \mathbf{A}_{m,m} \end{bmatrix} \begin{bmatrix} \boldsymbol{\sigma}_1 \\ \boldsymbol{\sigma}_2 \\ \vdots \\ \boldsymbol{\sigma}_m \end{bmatrix} = - \begin{bmatrix} \mathbf{v}_1 \\ \mathbf{v}_2 \\ \vdots \\ \mathbf{v}_m \end{bmatrix},$$

where each block $\mathbf{A}_{p,q}$ is of size $n \times n$. The diagonal blocks $\mathbf{A}_{p,p}$ are constructed using the technique described in Section 3.2. Next observe that in the off-diagonal blocks, the ‘‘naive’’ formula (10) works well since the kernel $G_\kappa(\mathbf{x}, \mathbf{x}')$ is smooth when \mathbf{x} and \mathbf{x}' belong to different scatterers.

Remark 3. *In this paper, we avoid considering the complications of scatterers that touch or are very close. The procedure described works well as long as the minimal distance between scatterers is not small compared to the resolution of the quadrature rules used. This means that if two scatterers are moderately close, high accuracy can be maintained by discretizing these two scatterers more finely.*

4. A BLOCK-DIAGONAL PRE-CONDITIONER FOR THE MULTIBODY SCATTERING PROBLEM

We solve the linear system (17) using the iterative solver GMRES [21], accelerated by a block-diagonal pre-conditioner. To formalize, let us decompose the system matrix as

$$\mathbf{A} = \mathbf{D} + \mathbf{B},$$

where

$$\mathbf{D} = \begin{bmatrix} \mathbf{A}_{1,1} & 0 & 0 & \cdots \\ 0 & \mathbf{A}_{2,2} & 0 & \cdots \\ 0 & 0 & \mathbf{A}_{3,3} & \cdots \\ \vdots & \vdots & \vdots & \ddots \end{bmatrix} \quad \text{and} \quad \mathbf{B} = \begin{bmatrix} 0 & \mathbf{A}_{1,2} & \mathbf{A}_{1,3} & \cdots \\ \mathbf{A}_{2,1} & 0 & \mathbf{A}_{2,3} & \cdots \\ \mathbf{A}_{3,1} & \mathbf{A}_{3,2} & 0 & \cdots \\ \vdots & \vdots & \vdots & \ddots \end{bmatrix}.$$

Then we use GMRES to solve the linear system

$$(18) \quad \boldsymbol{\sigma} + \mathbf{D}^{-1} \mathbf{B} \boldsymbol{\sigma} = -\mathbf{D}^{-1} \mathbf{v}.$$

We apply the matrix \mathbf{B} using the Fast Multipole Method [10, 4]; specifically the implementation [8] by Zydrunas Gimbutas and Leslie Greengard.

Remark 4. *The cost of evaluating the term $\mathbf{D}^{-1} \mathbf{B} \boldsymbol{\sigma}$ in (18) consists of two parts: applying \mathbf{B} to vector $\boldsymbol{\sigma}$ via FMM costs $O(mn)$ operations and applying the block-diagonal pre-conditioner costs $O(mn^{3/2})$ operations. Observe that the matrix \mathbf{D}^{-1} can be precomputed since each matrix $\mathbf{A}_{p,p}^{-1}$ is itself block-diagonal in the local Fourier basis, cf. formula (16). Applying $\mathbf{A}_{p,p}^{-1}$ to a vector $\mathbf{w} \in \mathbb{C}^n$ is executed as follows: (1) form \mathbf{Fw} using the FFT at cost $O(n \log n)$, (2) for each Fourier mode apply \mathbf{D}^{-1} to \mathbf{Fw} at cost $O(n^{3/2})$, and (3) use the FFT to apply \mathbf{F}^* to $\mathbf{D}^{-1} \mathbf{Fw}$.*

5. ACCELERATED MULTIBODY SCATTERING

In situations where the scatterers are not tightly packed, it is often possible to substantially reduce the size of the linear system (18) before applying an iterative solver. We use a technique that was introduced in [3] for problems in two dimensions, which exploits that when the scatterers are somewhat separated, the off-diagonal blocks $\mathbf{A}_{p,q}$ are typically rank deficient. Specifically, we assume that for some finite precision ε (say $\varepsilon = 10^{-10}$), each such block admits a factorization

$$(19) \quad \begin{array}{c} \mathbf{A}_{p,q} \\ n \times n \end{array} = \begin{array}{c} \mathbf{U}_p \\ n \times k \end{array} \begin{array}{c} \tilde{\mathbf{A}}_{p,q} \\ k \times k \end{array} \begin{array}{c} \mathbf{V}_q^* \\ k \times n \end{array} + \begin{array}{c} \mathbf{R}_{p,q} \\ n \times n \end{array}$$

where n is the number of nodes originally used to discretize a single scatterer, and k is the numerical rank of the factorization. The remainder term $\mathbf{R}_{p,q}$ satisfies $\|\mathbf{R}_{p,q}\| \leq \varepsilon$ in some suitable matrix norm (we typically use the Frobenius norm since it is simple to compute).

Now write the linear system (18) in block form as

$$(20) \quad \boldsymbol{\sigma}_p + \sum_{q \neq p} \mathbf{A}_{p,p}^{-1} \mathbf{A}_{p,q} \boldsymbol{\sigma}_q = -\mathbf{A}_{p,p}^{-1} \mathbf{v}_p, \quad p = 1, 2, 3, \dots, m.$$

We left multiply (20) by \mathbf{V}_p^* , and insert the factorization (19) to obtain

$$(21) \quad \mathbf{V}_p^* \boldsymbol{\sigma}_p + \sum_{q \neq p} \mathbf{V}_p^* \mathbf{A}_{p,p}^{-1} \mathbf{U}_p \tilde{\mathbf{A}}_{p,q} \mathbf{V}_q^* \boldsymbol{\sigma}_q = -\mathbf{V}_p^* \mathbf{A}_{p,p}^{-1} \mathbf{v}_p, \quad p = 1, 2, 3, \dots, m.$$

We now define quantities $\{\tilde{\boldsymbol{\sigma}}_p\}_{p=1}^m$, $\{\tilde{\mathbf{v}}_p\}_{p=1}^m$, and $\{\tilde{\mathbf{S}}_p\}_{p=1}^m$ via

$$(22) \quad \tilde{\boldsymbol{\sigma}}_p = \mathbf{V}_p^* \boldsymbol{\sigma}_p, \quad \tilde{\mathbf{v}}_p = \mathbf{V}_p^* \mathbf{A}_{p,p}^{-1} \mathbf{v}_p, \quad \mathbf{S}_{p,p} = \mathbf{V}_p^* \mathbf{A}_{p,p}^{-1} \mathbf{U}_p, \quad \text{for } p = 1, 2, 3, \dots, m.$$

Then the system (21) can be written

$$(23) \quad \tilde{\boldsymbol{\sigma}}_p + \sum_{q \neq p} \mathbf{S}_p \tilde{\mathbf{A}}_{p,q} \tilde{\boldsymbol{\sigma}}_q = -\tilde{\mathbf{v}}_p, \quad p = 1, 2, 3, \dots, m.$$

To write (23) in block form, we introduce matrices

$$(24) \quad \mathbf{S} = \begin{bmatrix} \mathbf{S}_1 & 0 & 0 & \cdots \\ 0 & \mathbf{S}_2 & 0 & \cdots \\ 0 & 0 & \mathbf{S}_3 & \cdots \\ \vdots & \vdots & \vdots & \ddots \end{bmatrix} \quad \text{and} \quad \tilde{\mathbf{B}} = \begin{bmatrix} 0 & \tilde{\mathbf{A}}_{1,2} & \tilde{\mathbf{A}}_{1,3} & \cdots \\ \tilde{\mathbf{A}}_{2,1} & 0 & \tilde{\mathbf{A}}_{2,3} & \cdots \\ \tilde{\mathbf{A}}_{3,1} & \tilde{\mathbf{A}}_{3,2} & 0 & \cdots \\ \vdots & \vdots & \vdots & \ddots \end{bmatrix},$$

whence equation (23) takes the form, cf. (18),

$$(25) \quad \tilde{\boldsymbol{\sigma}} + \tilde{\mathbf{S}} \tilde{\mathbf{B}} \tilde{\boldsymbol{\sigma}} = -\tilde{\mathbf{v}}.$$

The process of first forming the linear system (25), and then solving it using GMRES is very computationally efficient when the following techniques are used:

- The matrices $\{\mathbf{U}_p, \mathbf{V}_p\}_{p=1}^m$ in the factorizations (19) can be computed via a purely local procedure in $O(n^2k)$ operations, independent of the number of scatterers m . The idea is to use representation techniques from scattering theory to construct a local basis for all possible incoming harmonic fields (to within precision ε), see [11, Sec. 5.1] or [7, Sec. 6.2].
- In constructing the factorization (19), the so called *interpolatory decomposition* [3] should be used. Then each matrix \mathbf{U}_p and each matrix \mathbf{V}_p contains the $k \times k$ identity matrix \mathbf{I}_k . Specifically, there exists for each k an index vector $\tilde{I}_p \subset \{1, 2, \dots, n\}$ such that $\mathbf{U}(\tilde{I}_p, :) = \mathbf{V}(\tilde{I}_p, :) = \mathbf{I}_k$. Then each off-diagonal block $\tilde{\mathbf{A}}_{p,q}$ is given as a *submatrix* $\tilde{\mathbf{A}}_{p,q} = \mathbf{A}_{p,q}(\tilde{I}_p, \tilde{I}_q)$. In consequence, the matrix $\tilde{\mathbf{B}}$ is a sub-matrix of \mathbf{B} and can be rapidly applied using the FMM in $O(mk)$ operations.

- In evaluating the formula $\mathbf{S}_{p,p} = \mathbf{V}_p^* \mathbf{A}_{p,p}^{-1} \mathbf{U}_p$, we exploit that $\mathbf{A}_{p,p}^{-1}$ can be applied rapidly in Fourier space, cf. (16), to reduce the complexity of this step from $O(n^3)$ to $O(n^{3/2}k)$ if $\mathbf{A}_{p,p}^{-1}$ was precomputed and stored and to $O(n^2k)$ if $\mathbf{A}_{p,p}^{-1}$ is computed at this step.

Remark 5. *Efficient techniques for computing interpolative decompositions are described in [3]. More recently, techniques based on randomized sampling have proven to be highly efficient on modern computing platforms, in particular for problems in potential theory where the low-rank matrices to be approximated have very rapidly decaying singular values. We use the specific technique described in [12].*

6. NUMERICAL EXAMPLES

This section describes numerical experiments to assess the performance of the numerical scheme outlined in previous sections. All the experiments are carried out on a personal workstation with an Intel Xeon E-1660 3.3GHz 6-core CPU, and 128GB of RAM. The experiments explore (1) the accuracy of the algorithm, (2) the computational cost, (3) the performance of the block-diagonal pre-conditioner and (4) the performance of the acceleration scheme when scatterers are separated suitably. In all the experiments below, we measure accuracy against a known analytic solution u_{exact} . This solution is generated by randomly placing one point source inside each scatterer, and then solving (1) with the Dirichlet data v set to equal the field generated by these radiating sources. Let $\mathbf{u}_{\text{exact}}$ and $\mathbf{u}_{\text{approx}}$ denote the vectors holding the exact and the computed solutions at a set of 10 randomly chosen target points, placed at random on a sphere that is concentric to the smallest sphere holding all scatterers, but of twice the radius. The relative error, measured in the ℓ^∞ -norm, is then given by

$$E_\infty^{\text{rel}} = \frac{\|\mathbf{u}_{\text{approx}} - \mathbf{u}_{\text{exact}}\|_\infty}{\|\mathbf{u}_{\text{exact}}\|_\infty} = \frac{\max_i |\mathbf{u}_{\text{approx}}(i) - \mathbf{u}_{\text{exact}}(i)|}{\max_j |\mathbf{u}_{\text{exact}}(j)|}.$$

In addition to E_∞^{rel} , we report:

n	number of nodes discretizing each body (in form of $n = N_G \times N_F$, cf. Section 3.2)
N	total degree of freedom $N = m \times n$, where m is the number of scatterers
$N_{\text{compressed}}$	number of skeleton points after applying the compression scheme, cf. Section 5
T_{pre}	time (in seconds) of precomputation
T_{solve}	total time (in seconds) to solve for the surface charges σ via GMRES
T_{compress}	time (in seconds) to do compression in the accelerated scheme
I	number of GMRES iterations required to reduce the residual to 10^{-9} .

All the numerical experiments in this section are executed on domains composed of the three sample scatterers shown in Figure 3.

6.1. Laplace's equation. We first solve the Laplace equation exterior to the domains shown in Figures 4 and 5(a) (Examples 1 and 2, respectively). A combination of the single and double layer kernels is chosen to represent the potential outside the domain. The integral equation to be solved is

$$\frac{1}{2}\sigma(\mathbf{x}) + \int_\Gamma \frac{1}{4\pi} \left(\frac{1}{|\mathbf{x} - \mathbf{x}'|} + \frac{\mathbf{n}(\mathbf{x}') \cdot (\mathbf{x} - \mathbf{x}')}{|\mathbf{x} - \mathbf{x}'|^3} \right) \sigma(\mathbf{x}') dA(\mathbf{x}') = f(\mathbf{x}), \quad \mathbf{x} \in \Gamma.$$

6.1.1. Example 1. This example solves the exterior Laplace equation on the domain depicted in Figure 4. The domain consists of 125 ellipsoids contained in the box $[0, 10.2]^3$, where each ellipsoid has a major axis of length 2 and two minor axes of length 1. The minimal distance between any two ellipsoids is 0.05. We did not apply the compression technique since the scatterers are packed tightly. We compare the performance of the algorithm with and without using block-diagonal pre-conditioner in Table 1 and find that for this example, the pre-conditioning

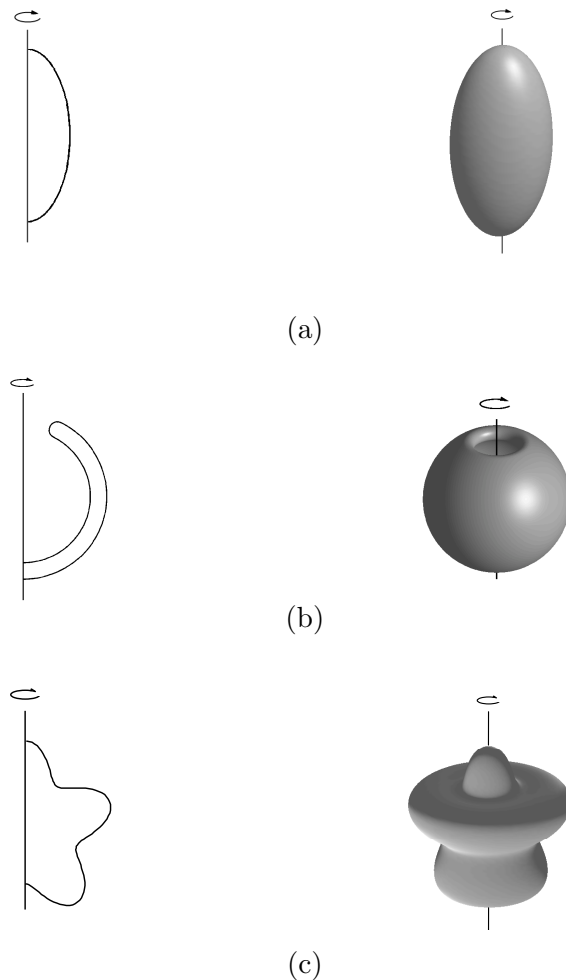


FIGURE 3. Domains used in the numerical examples. All items are rotated about their symmetry axis. (a) An ellipsoid. (b) A bowl-shaped cavity. (c) A starfish-shaped cavity.

does not make any real difference. The scheme quickly reaches 9 digits of accuracy with 10 100 discretization nodes per scatterer, with an overall solve time of about 40 minutes.

6.1.2. *Example 2.* This time the domain consists of 8 bowl-shaped cavities contained in the box $[0, 4.1]^3$ in Figure 5(a). The minimal distance between any two cavities is 0.5. Results are shown in Table 2. The scheme achieves 8 digits of accuracy with 400 discretization nodes on the generating curve and 201 Fourier modes. Again, the pre-conditioning is superfluous.

Remark 6. *All examples described in this section involve geometries where all the scatterers are copies of the basic shapes shown in Figure 3. In our experience, this restriction on the geometry does not in any way change the overall accuracy or efficiency of the solver. The only advantage we benefit from is that the pre-computation gets faster, as only a small number of scattering matrices need to be pre-computed. However, it is clear from the numbers given that even for a fully general geometry (without repetitions), the pre-computation time would be dominated by the time required for the FMM.*

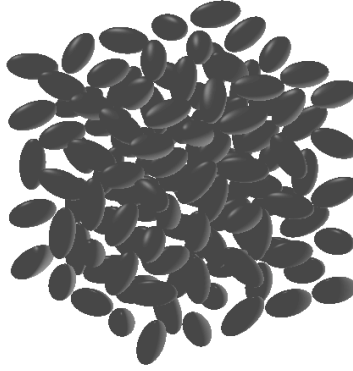


FIGURE 4. Domain contains 125 randomly oriented ellipsoids. Each ellipsoid has major axis of length 2, and the two minor axes are of length 1. The distance between any two ellipsoids is 0.05.

N	n	T_{pre}	I		T_{solve}		E_{∞}^{rel}
			(precond /no precond)	(precond /no precond)			
156 250	50×25	1.09e+00	31 /33	3.16e+02 /3.29e+02	9.731e-05		
312 500	100×25	3.44e+00	31 /33	6.84e+02 /6.82e+02	9.203e-05		
625 000	200×25	1.29e+01	31 /34	1.10e+03 /1.18e+03	9.814e-05		
318 750	50×51	1.53e+00	31 /33	6.29e+02 /7.44e+02	1.571e-06		
637 500	100×51	4.36e+00	31 /34	1.18e+03 /1.23e+03	1.529e-06		
1 275 000	200×51	1.36e+01	32 /34	2.70e+03 /2.53e+03	1.711e-06		
631 250	50×101	2.44e+00	31 /34	1.11e+03 /1.22e+03	2.165e-08		
1 262 500	100×101	6.11e+00	32 /34	2.45e+03 /2.60e+03	1.182e-09		

TABLE 1. (Example 1) Results from an exterior Laplace problem on the domain in Figure 4.

N	n	T_{pre}	I		T_{solve}		E_{∞}^{rel}
			(precond /no precond)	(precond /no precond)			
20 400	50×51	2.09e-01	398 /402	4.65e+02 /6.05e+02	1.251e-04		
40 800	100×51	4.55e-01	20 /23	4.94e+01 /6.09e+01	3.909e-05		
81 600	200×51	9.83e-01	20 /23	1.05e+02 /1.14e+02	3.164e-05		
40 400	50×101	2.25e-01	20 /23	4.72e+01 /6.17e+01	5.850e-05		
80 800	100×101	4.49e-01	20 /23	9.50e+01 /1.13e+02	1.627e-05		
161 600	200×101	1.35e+00	20 /24	2.05e+02 /2.39e+02	6.825e-06		
80 400	50×201	2.93e-01	20 /23	9.13e+01 /1.12e+02	5.704e-05		
160 800	100×201	7.05e-01	20 /24	1.96e+02 /2.40e+02	8.000e-06		
321 600	200×201	1.97e+00	20 /24	4.43e+02 /5.25e+02	1.931e-07		
643 200	400×201	5.78e+00	21 /24	7.68e+02 /8.19e+02	1.726e-08		

TABLE 2. (Example 2) Results from an exterior Laplace problem solved on the domain in Figure 5(a).

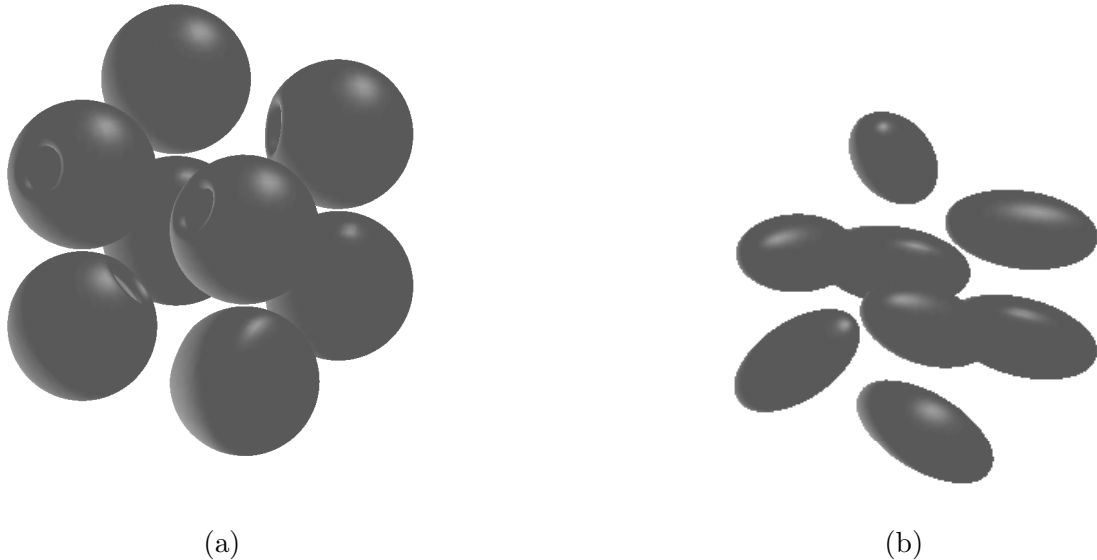


FIGURE 5. (a) Domain contains 8 bowl-shaped cavities. Distance between any two cavities is about half the radius of the bowls. (b) Domain contains 8 randomly oriented ellipsoids. The minimal distance between any two ellipsoids is $1/40$ of the length of the major axis.

6.2. Helmholtz Equation. We now consider the exterior Helmholtz problem (1). We represent the potential by a combination of the single and double layer kernels, see (3), and end up with the “combined field” integral equation (5).

6.2.1. Example 3. The domain in this experiment contains 8 ellipsoids in the box $[0, 4.05]^3$, whose minimal distance between any two is 0.05. The wavelength is 10π so that the scatterers are approximately 10 wavelengths in size and the whole region is about $20 \times 20 \times 20$ wavelengths in size. Results are presented in Table 3. We also compare the results without using block-diagonal pre-conditioner in the same table. Around twice of the iteration numbers are required resulting in twice of the computation time. Table 4 reports the results from an analogous experiment, but now the wavenumber increases such that each scatterer contains 20 wavelengths.

N	n	T_{pre}	I		T_{solve}		E_{∞}^{rel}
			(precond /no precond)	(precond /no precond)	(precond /no precond)	(precond /no precond)	
20 400	50×51	1.58e-01	35 /67		7.71e+02 /1.56e+03		1.364e-03
40 800	100×51	4.20e-01	36 /67		1.75e+03 /3.43e+03		1.183e-03
81 600	200×51	1.26e+00	36 /68		3.52e+03 /6.85e+03		1.639e-04
40 400	50×101	2.64e-01	36 /68		1.71e+03 /3.35e+03		1.312e-03
80 800	100×101	6.05e-01	36 /68		3.45e+03 /6.76e+03		1.839e-06
161 600	200×101	1.87e+00	37 /69		6.18e+03 /1.19e+04		5.126e-08
80 400	50×201	4.61e-01	36 /69		3.40e+03 /6.70e+03		1.312e-03
160 800	100×201	1.09e+00	37 /69		6.07e+03 /1.18e+04		1.851e-06
321 600	200×201	3.11e+00	37 /69		1.20e+04 /1.97e+04		1.039e-09

TABLE 3. (Example 3) Results from an exterior Helmholtz problem solved on the domain in Figure 5(b). Each ellipsoid is 10 wavelengths in diameter.

N	n	T_{pre}	I		T_{solve}		E_{∞}^{rel}
			(precond /no precond)	(precond /no precond)	(precond /no precond)	(precond /no precond)	
20 400	50×51	2.03e-01	58 /119	3.59e+03 /8.10e+03	4.362e+00		
40 800	100×51	4.44e-01	39 /102	3.98e+03 /1.11e+04	1.071e+00		
81 600	200×51	1.36e+00	39 /106	6.72e+03 /1.92e+04	1.008e+00		
40 400	50×101	2.78e-01	54 /94	5.43e+03 /1.02e+04	5.039e+00		
80 800	100×101	6.18e-01	36 /82	6.11e+03 /1.46e+04	8.919e-04		
161 600	200×101	1.93e+00	36 /83	9.44e+03 /2.32e+04	5.129e-07		
80 400	50×201	4.28e-01	55 /95	9.19e+03 /2.41e+04	5.031e+00		
160 800	100×201	1.07e+00	36 /83	9.49e+03 /2.31e+04	8.916e-04		
321 600	200×201	3.10e+00	37 /83	1.45e+04 /3.57e+04	8.781e-09		

TABLE 4. (Example 3) Results from an exterior Helmholtz problem, again solved on the domain in Figure 5(b), but now for a higher wave-number so that each ellipsoid is 20 wavelengths in diameter.

6.2.2. *Example 4.* This example solves the exterior Helmholtz problem on the cavity domain in Figure 5(a). Tables 5 and 6 show the results from experiments involving cavities of diameters 2 and 5 wavelengths, respectively. In this case, computing the actual scattering matrix for each scatterer was *essential*, without using these to pre-condition the problem, we did not observe any convergence in GMRES.

N	n	T_{pre}	I		T_{solve}		E_{∞}^{rel}
			(precond /no precond)	(precond /no precond)	(precond /no precond)	(precond /no precond)	
40 800	100×51	4.29e-01	59 /181	2.17e+03 /6.73e+03	1.127e-02		
81 600	200×51	1.28e+00	60 / -	4.23e+03 / -	1.131e-02		
80 800	100×101	6.83e-01	60 / -	4.18e+03 / -	3.953e-03		
161 600	200×101	1.90e+00	60 / -	8.93e+03 / -	3.802e-04		
323 200	400×101	6.07e+00	61 / -	1.91e+04 / -	3.813e-04		
160 800	100×201	1.09e+00	60 / -	8.35e+03 / -	4.788e-05		
321 600	200×201	3.07e+00	61 / -	1.88e+04 / -	5.488e-06		
643 200	400×201	9.61e+00	61 / -	4.03e+04 / -	8.713e-08		

TABLE 5. (Example 4) Results from an exterior Helmholtz problem solved on the domain in Figure 5(a). Each cavity is 2 wavelength in diameter.

6.3. **Accelerated scheme.** In this section, we provide two examples illustrating the efficiency of the accelerated scheme in Section 5 when applied to the geometries shown in Figures 6 (for the Laplace and Helmholtz equations) and 8 (for the Helmholtz equation). Recall that the idea here is to discretize each scatterer finely enough to fully resolve the local incoming and outgoing fields. This requires a somewhat large n number of points per scatterer, which for a system with m scatterers leads to a global coefficient matrix of size $nm \times nm$. Using the compression technique described in Section 5, we compute a “reduced” system of size $km \times km$, where now k is the (computed) rank of interaction between the scatterers. The number k is largely independent of the local geometry of a scatterer (an accurate upper bound can be derived by considering the speed of convergence when expanding the fundamental solution in terms of spherical harmonics). These examples illustrate representative sizes of k and n , and investigate whether the convergence of GMRES is affected by the compression.

N	n	T_{pre}	I		T_{solve}		E_{∞}^{rel}
			(precond /no precondition)		(precond /no precondition)		
80 800	100×101	6.54e-01	62 /304		5.17e+03 / 2.64e+04		1.555e-03
161 600	200×101	1.82e+00	63 / -		9.88e+03 / -		1.518e-04
323 200	400×101	6.46e+00	64 / -		2.19e+04 / -		3.813e-04
160 800	100×201	1.09e+00	63 / -		9.95e+03 / -		1.861e-03
321 600	200×201	3.00e+00	64 / -		2.19e+04 / -		2.235e-05
643 200	400×201	1.09e+01	64 / -		4.11e+04 / -		8.145e-06
641 600	200×401	5.02e+00	64 / -		4.07e+04 / -		2.485e-05
1 283 200	400×401	1.98e+01	65 / -		9.75e+04 / -		6.884e-07

TABLE 6. (Example 4) Results from an exterior Helmholtz problem solved on the domain in Figure 5(a). Now each cavity is 5 wavelengths in diameter.

6.3.1. *Example 5.* We apply the accelerated scheme in Section 5 to solve the Laplace’s equation on the domain exterior to the bodies depicted in Figure 6. This geometry contains $m = 50$ different shaped scatterers (ellipsoids, bowls, and rotated “starfish”) and is contained in the box $[0, 18] \times [0, 18] \times [0, 6]$. The minimal distance between any two bodies is 4.0. In this example, we have three different shapes of scatterers, and the relevant numbers n and k are given in Figure 7. The results obtained when solving the full $nm \times nm$ system are shown in Table 7, while the ones resulting from working with the compressed $km \times km$ system are shown in Table 8. We see that the compression did not substantially alter either the convergence speed of GMRES, or the final accuracy. Since the time for matrix-vector multiplications is dramatically reduced, the total solve time was reduced between one and two orders of magnitude.

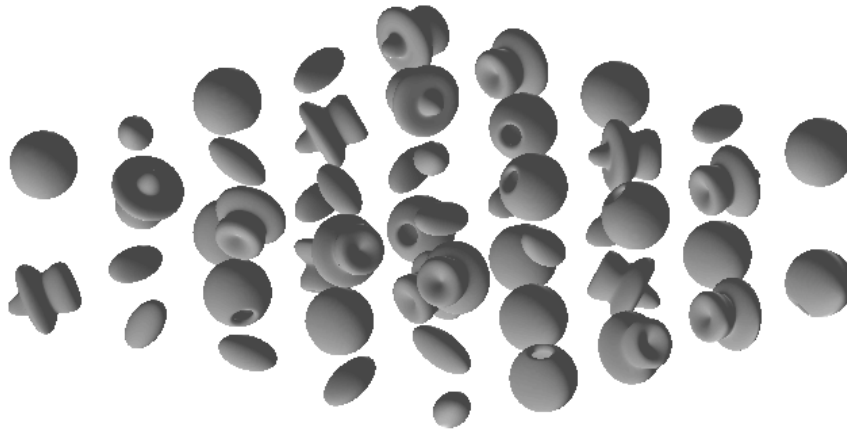


FIGURE 6. Domain contains 50 randomly oriented scatters.

6.3.2. *Example 6.* The accelerated scheme is applied to solve Helmholtz equation on domain containing 64 randomly placed ellipsoids depicted in Figure 8. The minimal distance between any two bodies is 6.0. Each ellipsoid is 5 wavelengths in diameter. The results for solving this problem without compression are given in Table 9, and with compression in Table 10. Again,

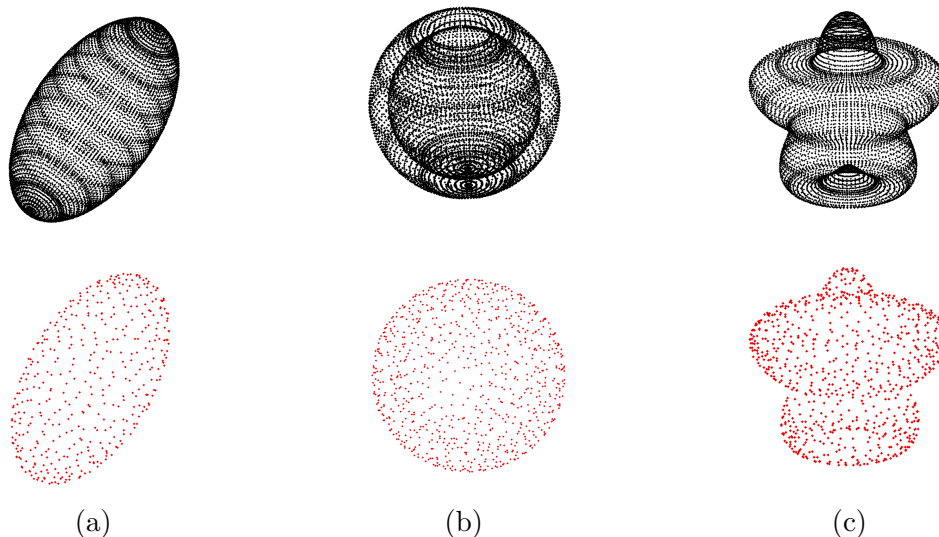


FIGURE 7. Example of skeletonization of three different scatterers before and after compression. With $n = 10\,100$ original discretization points (denoted by black dots), after compression (a) for an ellipsoid, only $k_a = 435$ points survive (denoted by red dots); (b) for a bowl-shaped cavity domain, only $k_b = 826$ points survive; (c) for a starfish-shaped cavity, only $k_c = 803$ points survive.

N	n	T_{pre}	I	T_{solve}	E_{∞}^{rel}
127 500	50×51	2.29e+00	18	1.52e+02	2.908e-05
255 000	100×51	4.70e+00	18	2.94e+02	2.329e-05
510 000	200×51	1.22e+01	18	5.85e+02	2.034e-05
252 500	50×101	3.23e+00	19	2.85e+02	3.677e-05
505 000	100×101	7.08e+00	19	5.29e+02	1.705e-06
1 010 000	200×101	1.93e+01	19	1.06e+03	4.128e-07
502 500	50×201	5.07e+00	19	5.02e+02	3.674e-05
1 050 000	100×201	1.28e+01	19	9.88e+02	1.673e-06
2 010 000	200×201	3.63e+01	19	2.07e+03	1.568e-08

TABLE 7. (Example 5) Results from solving an exterior Laplace problem on the domain in Figure 6 with $m = 50$ scatterers. Here the system with the full $nm \times nm$ coefficient matrix is solved (no compression).

we see that the convergence speed of GMRES is largely unaffected, and that the accelerated scheme is much faster.

6.3.3. *Example 7.* The accelerated scheme is applied to solve the Helmholtz equation on the domain in Figure 6. Each scatterer is two wavelengths in diameter. The results obtained when solving the original $nm \times nm$ system are given in Table 11, and the ones from the small $km \times km$ system are given in Table 12. The tables substantiate our claim regarding the efficiency of the acceleration scheme. Note that in Table 11, due to limitation of the memory, only estimations of the run time are reported when four million discretization nodes were used.

N	n	$N_{\text{compressed}}$	(k_a, k_b, k_c)	T_{compress}	I	T_{solve}	E_{∞}^{rel}
127 500	50×51	30 286	(411,797,746)	3.33e+01	18	3.85e+01	3.042e-05
255 000	100×51	33 876	(434,824,805)	7.00e+01	19	4.25e+01	1.458e-05
510 000	200×51	35 042	(449,847,838)	1.46e+02	19	4.26e+01	1.285e-05
252 500	50×101	32 186	(413,795,752)	6.66e+01	19	3.94e+01	3.008e-05
505 000	100×101	33 894	(435,826,803)	1.40e+02	19	4.04e+01	9.134e-06
1 010 000	200×101	35 094	(451,846,840)	3.20e+02	19	4.12e+01	5.287e-07
502 500	50×201	32 286	(414,797,754)	1.33e+02	19	3.98e+01	3.013e-05
1 050 000	100×201	33 798	(437,830,802)	3.00e+02	19	4.06e+01	9.130e-06
2 010 000	200×201	35 194	(453,848,842)	5.78e+02	19	4.21e+01	4.725e-08

TABLE 8. (Example 5) Results from solving an exterior Laplace problem on the domain in Figure 6 using the accelerated scheme with a reduced size coefficient matrix. The ranks k_a , k_b , and k_c for the three “species” of scatterers are given.

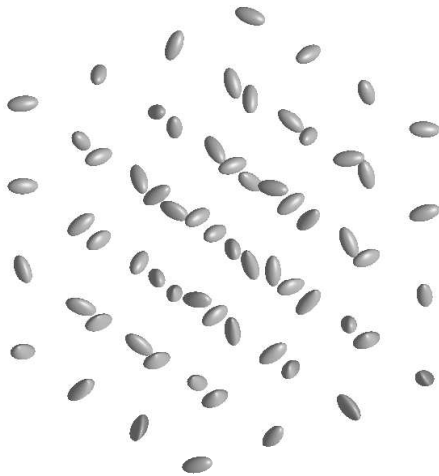


FIGURE 8. Domain contains $m = 64$ randomly oriented ellipsoids, where the minimal distance between any two is 6.0.

N	n	T_{init}	I	T_{solve}	E_{∞}^{rel}
80 000	50×25	4.41e-01	28	3.60e+03	7.009e-03
160 000	100×25	8.44e-01	28	5.69e+03	5.755e-03
163 200	50×51	8.22e-01	28	5.78e+03	1.239e-04
326 400	100×51	1.65e+00	29	8.75e+03	4.806e-05
652 800	200×51	3.36e+00	29	1.54e+04	5.552e-05
323 200	50×101	1.58e+00	29	8.64e+03	8.223e-06
646 400	100×101	3.24e+00	29	1.69e+04	1.354e-07
1 292 800	200×101	6.67e+00	29	3.01e+04	2.823e-08

TABLE 9. (Example 6) Results from solving an exterior Helmholtz problem on the domain in Figure 8 with $m = 64$ scatterers without compression (the system with the full $nm \times nm$ coefficient matrix is solved). Each ellipsoid is 5 wavelengths in diameter.

N	n	$N_{\text{compressed}}$	k	$T_{\text{compressed}}$	I	T_{solve}	E_{∞}^{rel}
80 000	50×25	61 184	956	1.92e+01	28	4.42e+03	2.339e-02
160 000	100×25	75 648	1182	6.58e+01	29	4.79e+03	8.656e-03
163 200	50×51	87 744	1371	8.50e+01	29	4.92e+03	2.798e-04
326 400	100×51	100 288	1567	2.83e+02	30	5.25e+03	5.892e-05
652 800	200×51	105 216	1644	9.06e+02	30	5.51e+03	6.056e-05
323 200	50×101	91 648	1432	2.40e+02	30	5.09e+03	9.485e-06
646 400	100×101	102 400	1552	8.55e+02	31	5.50e+03	2.150e-07
1 292 800	200×101	106 944	1671	2.91e+03	31	5.73e+03	8.441e-08

TABLE 10. (Example 6) Results from solving an exterior Helmholtz problem on the domain in Figure 8 using the accelerated scheme. Each ellipsoid is 5 wavelengths in diameter.

N	n	T_{init}	I	T_{solve}	E_{∞}^{rel}
252 500	50×101	5.33e+00	50	1.01e+04	3.211e-03
505 000	100×101	1.07e+01	50	2.04e+04	2.260e-03
1 010 000	200×101	2.21e+01	51	4.16e+04	8.211e-04
502 500	50×201	1.02e+01	51	2.15e+04	8.273e-03
1 005 000	100×201	2.01e+01	51	4.20e+04	3.914e-03
2 010 000	200×201	3.90e+01	51	8.42e+04	5.044e-06
4 020 000	400×201	–	–	~ 48h	–
2 005 000	100×401	3.89e+01	51	8.30e+04	4.244e-04
4 010 000	200×401	–	–	~ 48h	–

TABLE 11. (Example 7) Results from solving the exterior Helmholtz problem on the domain in Figure 6 with $m = 50$ scatterers, using the full $nm \times nm$ coefficient matrix (no compression). Each scatterer is 2 wavelengths in diameter.

N	n	$N_{\text{compressed}}$	(k_a, k_b, k_c)	$T_{\text{compressed}}$	I	T_{solve}	E_{∞}^{rel}
252 500	50×101	53 390	(775,1254,1211)	2.26e+02	52	2.48e+03	4.941e-03
505 000	100×101	57 934	(823,1358,1337)	5.17e+02	53	2.72e+03	2.026e-03
1 010 000	200×101	60 512	(856,1420,1399)	1.14e+03	54	2.89e+03	4.865e-04
502 500	50×201	54 538	(789,1283,1238)	4.89e+02	53	2.63e+03	9.276e-03
1 005 000	100×201	59 036	(838,1384,1363)	1.10e+03	54	2.90e+03	4.392e-03
2 010 000	200×201	61 488	(872,1443,1419)	2.70e+03	56	3.10e+03	7.709e-06
4 020 000	400×201	61 664	(888,1428,1427)	1.50e+04	57	3.31e+03	1.856e-06
2 005 000	100×401	60 106	(853,1409,1388)	2.58e+03	56	3.04e+03	9.632e-04
4 010 000	200×401	61 818	(885,1441,1427)	1.54e+04	57	3.32e+03	2.452e-07

TABLE 12. (Example 7) Results from solving an exterior Helmholtz problem on the domain in Figure 6 using the accelerated scheme with a reduced size coefficient matrix. Each scatterer is 2 wavelengths in diameter. The ranks k_a , k_b , and k_c , for each of the three types of scatterer is given.

7. CONCLUSIONS AND FUTURE WORK

We have presented a highly accurate numerical scheme for solving acoustic scattering problems on domains involving multiple scatterers in three dimensions, under the assumption that each

scatterer is axisymmetric. The algorithm relies on a boundary integral equation formulation of the scattering problem, combined with a highly accurate Nyström discretization technique. For each scatterer, a scattering matrix is constructed via an explicit inversion scheme. Then these individual scattering matrices are used as a block-diagonal pre-conditioner to GMRES to solve the very large system of linear equations. The Fast Multiple Method is used to accelerate the evaluation of all inter-body interactions. Numerical experiments show that while the block-diagonal pre-conditioner does not make almost any difference for “zero-frequency” scattering problems (governed by Laplace’s equation), it dramatically improves the convergence speed at intermediate frequencies.

Furthermore, for problems where the scatterers are well-separated, we present an accelerated scheme capable of solving even very large scale problems to high accuracy on a basic personal work station. In one numerical example in Section 6, the numbers of degrees of freedom required to solve the Laplace equation to eight digits of accuracy on a complex geometry could be reduced by a factor of 57 resulting in a reduction of the total computation time from 35 minutes to 10 minutes (9 minutes for compression and 42 seconds for solving the linear system). For a Helmholtz problem the reduction of computation time is even more significant: the numbers of degrees of freedom to reach seven digits of accuracy was in one example reduced by a factor of 65; consequently the overall computation time is reduced from 48 hours to 5 hours (4 hours for compression and 1 hour for solving the linear system).

The scheme presented assumes that each scatterer is rotationally symmetric; this property is used both to achieve higher accuracy in the discretization, and to accelerate all computations (by using the FFT in the azimuthal direction). It appears conceptually straight-forward to use the techniques of [1, 14] to generalize the method presented to handle scatterers with edges (generated by “corners” in the generating curve). The idea is to use local refinement to resolve the singular behavior of solutions near the corner, and then eliminate the added “superfluous” degrees of freedom added by the refinement via a local compression technique, see [6].

Acknowledgements: The research reported was supported by the National Science Foundation under contracts 1320652, 0941476, and 0748488, and by the Defense Advanced Projects Research Agency under the contract N66001-13-1-4050.

REFERENCES

- [1] James Bremer, *On the nyström discretization of integral equations on planar curves with corners*, Applied and Computational Harmonic Analysis **32** (2012), no. 1, 45–64.
- [2] James Bremer, Adrianna Gillman, and Per-Gunnar Martinsson, *A high-order accurate accelerated direct solver for acoustic scattering from surfaces*, 2013, To appear in *BIT Numerical Analysis*, arXiv preprint arXiv:1308.6643.
- [3] H. Cheng, Z. Gimbutas, P.G. Martinsson, and V. Rokhlin, *On the compression of low rank matrices*, SIAM Journal of Scientific Computing **26** (2005), no. 4, 1389–1404.
- [4] Hongwei Cheng, William Y. Crutchfield, Zydrunas Gimbutas, Leslie F. Greengard, J. Frank Ethridge, Jingfang Huang, Vladimir Rokhlin, Norman Yarvin, and Junsheng Zhao, *A wideband fast multipole method for the Helmholtz equation in three dimensions*, J. Comput. Phys. **216** (2006), no. 1, 300–325.
- [5] D. Colton and R. Kress, *Inverse acoustic and electromagnetic scattering theory*, 2nd ed., Springer-Verlag, New York, 1998.
- [6] A Gillman, S Hao, and PG Martinsson, *Short note: A simplified technique for the efficient and highly accurate discretization of boundary integral equations in 2d on domains with corners*, Journal of Computational Physics **256** (2014), 214–219.
- [7] Adrianna Gillman, Patrick Young, and Per-Gunnar Martinsson, *A direct solver $o(n)$ complexity for integral equations on one-dimensional domains*, Frontiers of Mathematics in China **7** (2012), 217–247, 10.1007/s11464-012-0188-3.
- [8] Z. Gimbutas and L. Greengard, *FMMLIB3D, fortran libraries for fast multiple method in three dimensions*, 2011, <http://www.cims.nyu.edu/cmcl/fmm3dlib/fmm3dlib.html>.

- [9] Zydrunas Gimbutas and Leslie Greengard, *Fast multi-particle scattering: A hybrid solver for the maxwell equations in microstructured materials.*, J. Comput. Physics **232** (2013), no. 1, 22–32.
- [10] L. Greengard and V. Rokhlin, *A fast algorithm for particle simulations*, J. Comput. Phys. **73** (1987), no. 2, 325–348.
- [11] Leslie Greengard, Denis Gueyffier, Per-Gunnar Martinsson, and Vladimir Rokhlin, *Fast direct solvers for integral equations in complex three-dimensional domains*, Acta Numer. **18** (2009), 243–275.
- [12] N. Halko, P. G. Martinsson, and J. A. Tropp, *Finding structure with randomness: probabilistic algorithms for constructing approximate matrix decompositions*, SIAM Rev. **53** (2011), no. 2, 217–288.
- [13] S. Hao, A.H. Barnett, P.G. Martinsson, and P. Young, *High-order accurate methods for nystrom discretization of integral equations on smooth curves in the plane*, Advances in Computational Mathematics **40** (2014), no. 1, 245–272.
- [14] J. Helsing and R. Ojala, *Corner singularities for elliptic problems: Integral equations, graded meshes, quadrature, and compressed inverse preconditioning*, Journal of Computational Physics **227** (2008), no. 20, 8820–8840.
- [15] K.L. Ho and L. Greengard, *A fast direct solver for structured linear systems by recursive skeletonization*, SIAM Journal on Scientific Computing **34** (2012), no. 5, 2507–2532.
- [16] P. Kolm and V. Rokhlin, *Numerical quadratures for singular and hypersingular integrals*, Comput. Math. Appl. **41** (2001), 327–352.
- [17] A.H. Kuijpers, G. Verbeek, and J.W. Verheij, *An improved acoustic fourier boundary element method formulation using fast fourier transform integration*, J. Acoust. Soc. Am. **102** (1997), 1394–1401.
- [18] P.G. Martinsson and V. Rokhlin, *A fast direct solver for boundary integral equations in two dimensions*, J. Comput. Phys. **205** (2004), 1–23.
- [19] Jean-Claude Nédélec, *Acoustic and electromagnetic equations: Integral representations for harmonic functions*, Springer, New York, 2012.
- [20] F.J. Rizzo and D.J. Shippy, *A boundary integral approach to potential and elasticity problems for axisymmetric bodies with arbitrary boundary conditions*, Mech. Res. Commun. **6** (1979), 99–103.
- [21] Youcef Saad and Martin H Schultz, *Gmres: A generalized minimal residual algorithm for solving nonsymmetric linear systems*, SIAM Journal on scientific and statistical computing **7** (1986), no. 3, 856–869.
- [22] A. F. Seybert, B. Soenarko, F. J. Rizzo, and D. J. Shippy, *A special integral equation formulation for acoustic radiation and scattering for axisymmetric bodies and boundary conditions*, The Journal of the Acoustical Society of America **80** (1986), no. 4.
- [23] B. Soenarko, *A boundary element formulation for radiation of acoustic waves from axisymmetric bodies with arbitrary boundary conditions*, J. Acoust. Soc. Am. **93** (1993), 631–639.
- [24] S.V. Tsinopoulos, J.P. Agnantiaris, and D. Polyzos, *An advanced boundary element/fast fourier transform axisymmetric formulation for acoustic radiation and wave scattering problems*, J. Acoust. Soc. Am. **105** (1999), 1517–1526.
- [25] W. Wang, N. Atalla, and J. Nicolas, *A boundary integral approach for accoustic radiation of axisymmetric bodies with arbitrary boundary conditions valid for all wave numbers*, J. Acoust. Soc. Am. **101** (1997), 1468–1478.
- [26] P. Young, S. Hao, and P. G. Martinsson, *A high-order nystrom discretization scheme for boundary integral equations defined on rotationally symmetric surfaces*, J. Comput. Phys. **231** (2012), no. 11, 4142–4159.